AGU PUBLICATIONS

Geophysical Research Letters

RESEARCH LETTER

10.1002/2014GL062454

Key Points:
- NAME distal ash layer depths compare exceptionally well with observations
- Ash layer depth is determined by vertical wind shear and turbulent mixing
- The volcano characteristics have a minor effect on distal ash layer depths

Correspondence to:
H. F. Dacre,
h.f.dacre@reading.ac.uk

Citation:
Dacre, H. F., A. L. M. Grant, N. J. Harvey, D. J. Thomson, H. N. Webster, and F. Marenco (2015), Volcanic ash layer depth: Processes and mechanisms, *Geophys. Res. Lett.*, *42*, 637–645, doi:10.1002/2014GL062454.

Received 5 NOV 2014
Accepted 24 DEC 2014
Accepted article online 29 DEC 2014
Published online 26 JAN 2015

Volcanic ash layer depth: Processes and mechanisms

H. F. Dacre[1], A. L. M. Grant[1], N. J. Harvey[1], D. J. Thomson[2], H. N. Webster[2], and F. Marenco[2]

[1]Department of Meteorology, University of Reading, Reading, UK, [2]Met Office, Exeter, UK

Abstract The long duration of the 2010 Eyjafjallajökull eruption provided a unique opportunity to measure a widely dispersed volcanic ash cloud. Layers of volcanic ash were observed by the European Aerosol Research Lidar Network with a mean depth of 1.2 km and standard deviation of 0.9 km. In this paper we evaluate the ability of the Met Office's Numerical Atmospheric-dispersion Modelling Environment (NAME) to simulate the observed ash layers and examine the processes controlling their depth. NAME simulates distal ash layer depths exceptionally well with a mean depth of 1.2 km and standard deviation of 0.7 km. The dominant process determining the depth of ash layers over Europe is the balance between the vertical wind shear (which acts to reduce the depth of the ash layers) and vertical turbulent mixing (which acts to deepen the layers). Interestingly, differential sedimentation of ash particles and the volcano vertical emission profile play relatively minor roles.

1. Introduction

The disruption of air travel as a result of the 2010 Icelandic Eyjafjallajökull eruption brought attention to the serious global economic consequences of widely dispersed volcanic ash clouds. The unusually long duration of the eruption provided many opportunities to measure the resulting ash cloud that spread over the North Atlantic and Europe. Layers of concentrated ash were observed exhibiting a high degree of spatial and temporal variability [*Marenco et al.*, 2011; *Pappalardo et al.*, 2013; *Grant et al.*, 2013; *Schumann et al.*, 2011]. This paper aims to evaluate our ability to model the depth of these layers.

Research and commercial aircraft measuring vertical profiles of other atmospheric aerosols (e.g., dust and smoke) and chemical constituents (e.g., ozone and water vapour) frequently discern similar quasi-horizontal atmospheric layers to the volcanic ash layers observed during the Eyjafjallajökull eruption [*Newell et al.*, 1996; *Stoller et al.*, 1999]. Layering is so ubiquitous that it is estimated that up to one fifth of the lowest 12 km of the atmosphere can be occupied by such layers at any given time depending on the region and the season [*Newell et al.*, 1999; *Thouret et al.*, 2000]. It has been found that the processes affecting the depth of aerosol and chemical layers include spatial variations in the speed and direction of atmospheric winds (particularly vertical variations) [*Haynes and Anglade*, 1997; *Newell et al.*, 1999; *Colette and Ancellet*, 2006], mixing due to 3-D turbulent eddies, and gravitational settling of aerosols [*Rose et al.*, 2000; *Colette and Ancellet*, 2006]. Additionally, for volcanic eruptions, the eruptive plume dynamics can also lead to the formation of layers. In the absence of a strong crosswind, intense volcanic plumes typically form a radially spreading umbrella cloud layer near the top of the eruption column at its level of neutral buoyancy [*Sparks et al.*, 1997]. In this paper we will determine which of these processes dominated the formation of the ash layers observed over Europe during the 2010 Eyjafjallajökull eruption.

2. NAME Model Simulations

The model used in this study is the Numerical Atmospheric-dispersion Modelling Environment (NAME). NAME is a Lagrangian particle trajectory model [*Jones et al.*, 2007]. It is the model used by the London Volcanic Ash Advisory Centre to produce advisories on the extent of volcanic ash in the atmosphere. In these simulations emission of volcanic ash is modeled by releasing 20 million model particles, with each model particle representing a mass of volcanic ash. The model ash particles are carried along by the wind with turbulent mixing represented by giving the trajectories a stochastic perturbation. In this paper, NAME III (version 6.3) is driven using the 3-D winds and thermodynamic fields from the Met Office global numerical weather prediction model, using analysis fields updated every 6 h interspersed with short period forecast fields, giving a time resolution of 3 h. Ash concentrations are computed by summing the mass of ash particles in areas of 0.375° latitude by 0.5625° longitude, averaged over 100 m in the vertical and over a time period of 1 h.

Several eruption source parameters (ESPs) must be specified to characterize the volcanic emission. The ESPs are the following: plume rise height, vertical ash emission profile, particle size distribution, ash density, and mass eruption rate. The plume rise height input is taken from measurements provided by the Icelandic Meteorological Office's C band radar [*Arason et al.*, 2011]. The ash emission profile represents the vertical distribution of ash mass released in the column above the volcano vent. For the simulations in this study, the emission profile is uniform over a specified depth extending down from the plume rise height. The particle size distribution specifies the mass fraction of ash in six different particle size bins. It represents the particle size distribution at a distance from the source at which large unaggregated particles and aggregates with diameter $>$ 100 μm have been removed from the plume via sedimentation. In these simulations the particle size distribution is specified using the best match to in situ observations for the Eyjafjallajökull eruption [*Dacre et al.*, 2013], and the ash density is assumed to be 2300 kg m^{-3}. The mass eruption rate is specified using the plume rise height relationship given in *Dacre et al.* [2011].

3. Lidar Observations

In this paper, we shall make use of the European Aerosol Research Lidar Network (EARLINET) database available at www.earlinet.org [*Pappalardo et al.*, 2013]. EARLINET includes 27 lidar stations, distributed over Europe operating with vertical resolutions between 60 and 180 m. From 15 April to 1 May 2010 more than 1000 h of measurements were taken. During this period the method described in *Mona et al.* [2012] for identifying volcanic ash layers was applied at all the EARLINET stations. For each layer, center of mass altitudes are reported together with maximum backscatter and column-integrated backscatter. As much of the scientific literature for this event has focused on specific times and/or locations, the EARLINET observations represents a unique data set for extended spatial and temporal model evaluation such as demonstrated in this paper.

4. Ash Layer Depth Methodology

To make comparisons between the observed and modeled ash layer depths, it is useful to have a measure of the depth of an ash layer which does not depend on the detailed shape of the vertical concentration profile. The ratio of the column-integrated ash loading/backscatter to the maximum concentration/backscatter is used as an effective depth, l_{eff}, for the modeled and lidar measurements, respectively.

Between 00Z on 15 April and 00Z on 1 May 2010, 1001 ash profiles were observed by the EARLINET lidars. For comparison, as ash is often mixed with boundary layer pollution and, as such, is excluded by the EARLINET lidar ash layer detection algorithm, a minimum height threshold of 1250 m was applied to the modeled profiles. This results in an 8% reduction in the number of model profiles. Following this, a second step was applied in which NAME layers with maximum concentrations $<$ 25 μg m^{-3} were removed. This step avoids biasing the model results by including profiles with virtually no ash mass. Note that while this is a very low threshold, it is sufficient to remove a further 16% of the (nonzero) NAME profiles, virtually all of which (95%) have ash layer depths $<$ 1 km deep. Following these threshold constraints, between 00Z on 15 April and 00Z on 1 May 2010, 6042 NAME profiles were extracted at the lidar locations. There are many more modeled ash layers than observed because not all of the lidars were operating continuously for the entire period and because the EARLINET lidar ash layer detection algorithm also excludes ash layers that are mixed with meteorological cloud, Saharan dust, or soot from forest fires.

5. Results

First, we compare NAME ash layer depths to the EARLINET observations for simulations in which the ESPs (emission profile, particle size distribution) and vertical subgrid-scale mixing are as specified for the control NAME simulation described in Table 1.

Figures 1a and 1b show maps of the NAME-simulated ash cloud layer depth and (center of mass) height, respectively, at 00Z on 17 April 2010. As described in *Dacre et al.* [2011], ash emitted from the volcano between 14 and 16 April was advected anticyclonically, toward Europe, around a high-pressure system centered to the west of the UK. After 24 h the ash cloud began to diverge, and transport occurred both northeastward and southwestward, parallel to a cold front. The NAME ash layers exhibit a high degree of

Table 1. Characteristics of the NAME Simulations[a]

NAME Simulation	Emission Profile (km)	PSD (Mode) (μm)	Turbulence ($m^2 s^{-1}$)
Control	1	3–10	1
Thick emission	**3**	3–10	1
Thin emission	**0.25**	3–10	1
Heavy PSD	1	**10–30**	1
Light PSD	1	**0.3–3**	1
High turbulence	1	3–10	**9**
Low turbulence	1	3–10	**0.0001**

[a]Emission profile represents the depth over which particles are emitted at the source in a uniform distribution below the plume top. PSD (mode) denotes the mode of the particle size distribution, and the full size distribution is described in Table 2. Turbulence represents the vertical subgrid diffusion due to turbulent mixing by unresolved eddies. Different values used in each simulation are highlighted in bold.

spatial variability with ash layer depths ranging from 100 m to 3 km (Figure 1a) and ash layer heights ranging from 1 to 10 km (Figure 1b). In this snapshot of the ash cloud, the ash layer depth, within the center of the plume, increases from approximately 1000 m at the volcano source (consistent with the source emission profile) to around 1750 m as it travels toward Europe. This is due to the influence of processes which act to deepen the ash layer (subgrid-scale mixing and differential sedimentation) and processes which act to reduce the depth of the ash layer (vertical wind shear). Here we use differential sedimentation to describe the process by which larger particles fall faster than smaller particles, thus leading to an increase in the vertical distribution of ash particles. The effect of vertical wind shear can be seen in Figure 1b, where strong gradients of ash layer height exist, for example, over northwest Europe. Vertical wind shear acts to create a vertically sloped ash layer extending from 6 km down to 1 km. This vertically sloped ash layer was observed over many sites in the UK and Europe at this time [e.g., *Flentje et al.*, 2010; *Marenco and Hogan*, 2011; *Ansmann et al.*, 2011; *Dacre et al.*, 2011; *Devenish et al.*, 2012].

5.1. Can NAME Simulate the Vertical Depth of the Observed Ash Clouds?

Figure 2a shows the frequency of the 1001 ash layer depth measurements observed during the period 15 April to 1 May 2010. The observed ash layer depths range from 0.1 km to 4.5 km with a mean of 1.2 km and a standard deviation of 0.9 km. This is consistent with the results of *Schumann et al.* [2011] who observed depths ranging from 0.1 to 3 km and that found by *Marenco et al.* [2011] who observed layer depths between 0.5 and 2.9 km over the UK. However, it should be noted that the definition of ash layer depth and the periods and locations over which the ash layers were observed varies in these studies, so a direct comparison is not possible.

Figure 2a also shows the frequency of the 6042 NAME-simulated ash layer depth measurements extracted at the lidar locations. The distribution of ash layer depths in NAME is closely comparable to the observations (mean 1.2 km and standard deviation 0.7 km) suggesting that NAME can simulate ash layer depths that are consistent with those observed. It should be noted that volcanic ash cloud simulations produced at

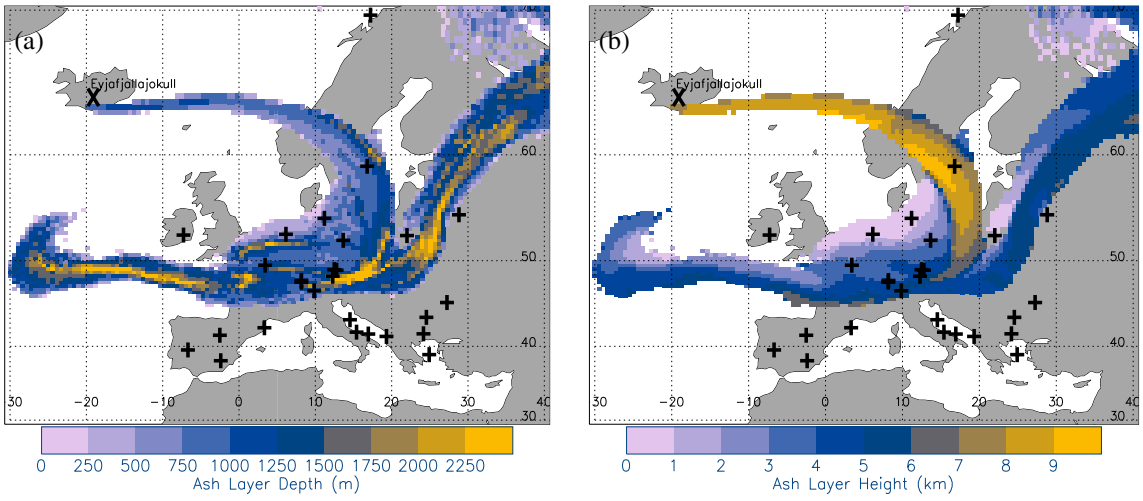

Figure 1. Maps of the NAME-simulated ash cloud at 00Z on 17 April 2010. (a) Ash layer depth (m) and (b) ash layer height above ground level (km). Crosses show the locations of the EARLINET lidars and Eyjafjallajökull volcano.

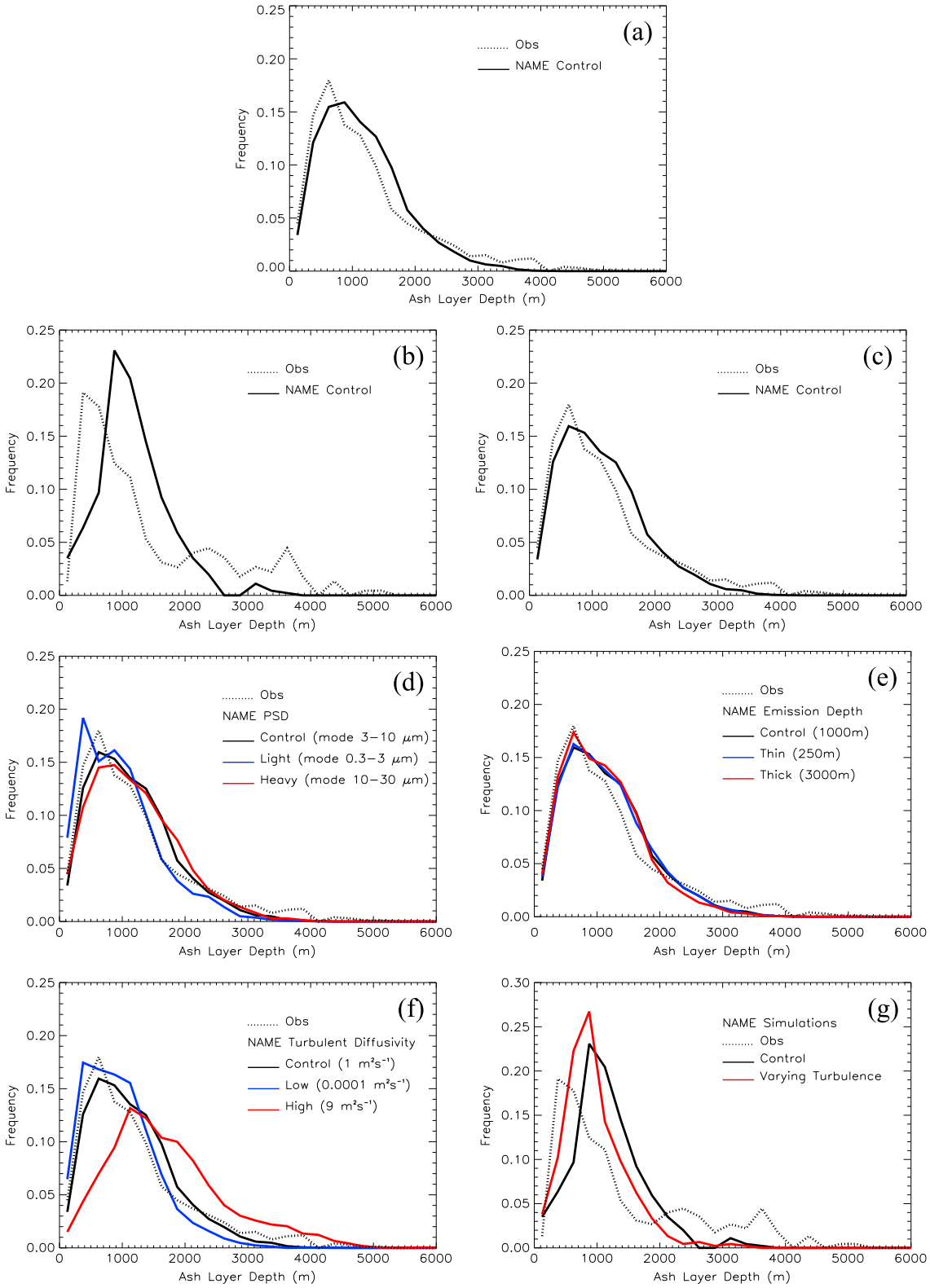

Figure 2. Relative frequency of ash layer depth (m): (a) 15 April to 1 May 2010, (b and g) 15–17 April 2010, and (c–f) 18 April to 1 May 2010. EARLINET observed (dotted). NAME simulations from the control (Figures 2a–2c) and with varying particle size distribution (PSD) (Figure 2d), varying source emission profile (Figure 2e), varying free-tropospheric vertical turbulent diffusion (Figure 2f), and with inclusion of a space-time-varying turbulence scheme (Figure 2g).

Table 2. Particle Size Distributions Used in the NAME Simulations Described in Table 1

	Light PSD (0.3–3 μm)	Control (3–10 μm)	Heavy PSD (10–30 μm)
Diameter (μm)	Fraction of Mass (%)	Fraction of Mass (%)	Fraction of Mass (%)
0.1–0.3	0	0	0.1
0.3–1.0	50	1	0.5
1.0–3.0	50	31	5
3.0–10.0	0	59	20
10.0–30.0	0	9	70
30.0–100.0	0	0	4.4

lower vertical resolution than that used in these simulations results in a shift in the frequency distribution to deeper ash layer depths. The mean increases from 1.2 km to 2.6 km when the vertical resolution increases from 100 m to 2000 m, reflecting the inability of the model to resolve the shallowest ash layers at low resolution. However, increasing the vertical resolution of the model output by a factor of N requires an equivalent increase in the number of particles used in the simulation to avoid creating noisy concentration fields. Therefore, the model takes about N times longer to run.

In the NAME simulation the standard deviation of ash layer depths is slightly lower than that found in the observations. This is because compared to the observations, the relative frequencies of very shallow ash layers (<500 m deep) and very deep ash layer depths (>2500 m deep) are underpredicted. Figures 2b and 2c show the ash layer depth for the periods 15–17 April and 18 April to 1 May, respectively. There are 225 observed (mean 1.4 km and standard deviation 1.1 km) and 455 model profiles (mean 1.2 km and standard deviation 0.6 km) during the early period of the eruption (15–17 April). A large fraction of the very shallow and very deep layers observed during April occurred during this early stage of the eruption. There are 776 observed profiles (mean 1.1 km and standard deviation 0.8 km) and 5587 modeled profiles (mean 1.2 km and standard deviation 0.7 km) during the later part of April (18 April to 1 May). NAME captures the distribution of ash layer depths remarkably well during this later period. Given the excellent agreement between the NAME-simulated and observed ash layer depths for the period 18 April to 1 May 2010, we now use NAME to investigate the dominant controls on ash layer depth during this period. We return to discuss the earlier period in section 5.3.

5.2. What Controls the Depth of Volcanic Ash Layers?

In the NAME simulations to be presented in this section, the ash layer depths simulated by NAME using the control run eruption source parameters and vertical subgrid-scale mixing (Table 1) are compared to simulations in which the emission profile is varied (to test sensitivity to the source characteristics), the particle size distribution is varied (to test sensitivity to the spreading effect of differential sedimentation), and the free-tropospheric vertical turbulent diffusion is varied (to test sensitivity to vertical subgrid mixing by unresolved turbulent eddies). The values used in these simulations are given in Table 1 and are chosen to represent plausible upper and lower bounds.

Figures 2d–2f show the ash layer depths during the period 18 April to 1 May only. Figure 2d shows the ash layer depths using different particle size distributions (PSD). The light PSD simulation produces slightly shallower ash clouds than the control simulation while the heavy PSD simulation produces a wider range of ash layer depths as a result of a wider range of sedimentation velocities (produced by the range of particle sizes in this distribution 0.3–100 μm; see Table 2). The ash cloud depth distributions using the light and heavy PSD's are, however, similar to the control simulation. It should be noted that using an even lighter PSD does not reduce the ash layer depths further as the sedimentation rate of particles with diameters < 3 μm is negligible. Similarly, using a heavier PSD does not increase the ash layer depths further as the sedimentation rate of particles with diameters $>$ 30 μm is such that these particles have largely been deposited to the surface before reaching the EARLINET lidars. Therefore, during this period, the size of the ash particles emitted from the volcano does not appear to modify the distribution of ash layer depths greatly.

Figure 2e shows the ash layer depth distribution simulated by NAME using different source emission profiles. During the period 18 April to 1 May the plume rise height varies between 3.0 km and 4.5 km. The thin emission profile (250 m deep) and thick emission profile (3000 m deep) produce very similar ash layer depth distributions to the control emission profile (1000 m deep). This is because the wind shear acting on

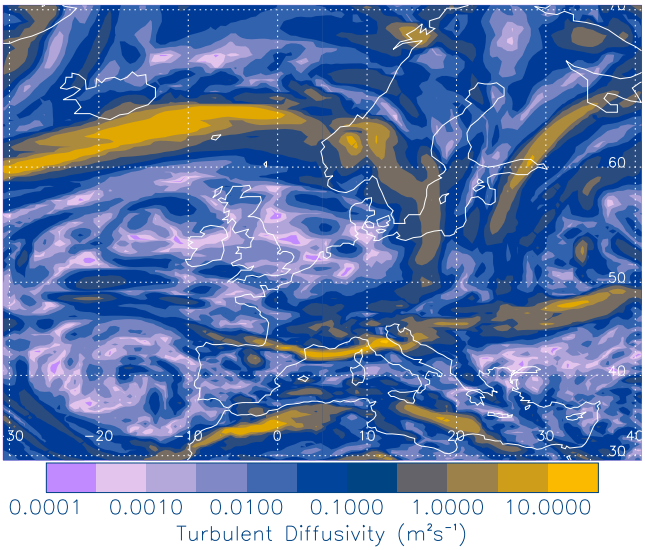

Figure 3. Space-time-varying vertical turbulent eddy diffusivity at 00Z on 17 April 2010 at an altitude of 6 km. For comparison, the NAME control simulation uses a constant vertical turbulent eddy diffusivity of 1 $m^2\ s^{-1}$.

the thick emission profile is greater than that acting on the thin emission profile, resulting in more widely spread ash layers. This interesting result shows that the emission profile is not the dominant mechanism determining the depth of the observed ash layers for the Eyjafjallajökull volcano, at least at distances (>3000 km) from the volcano in Europe.

Figure 2f shows the ash layer depth distributions using different turbulence values. Increasing the vertical mixing increases the ash layer depths while decreasing the vertical mixing leads to a reduction in ash layer depths. Thus, it appears that it is the competing effects of subgrid-scale mixing and vertical wind shear rather than the volcano source characteristics (emission profile and particle size distribution) which dominates the depth of the simulated ash clouds during the period 18 April to 1 May 2010. While it is important to specify the eruption source parameters correctly to capture the height of the ash cloud, the location of the ash cloud downwind, and the structure of ash clouds close to the source, at distances sufficiently downwind from the source atmospheric processes control ash layer depths at least for this specific case.

5.3. What Causes the Very Shallow and Deep Ash Layer Depths?

As shown in Figure 2b, ash layer depths shallower than 1 km and greater than 3 km deep were observed during the early stage of the Eyjafjallajökull eruption. These very shallow and deep ash layers were not well captured by the NAME model. The results in section 5.2 suggest that this may be due to an overestimation or underestimation of subgrid-scale mixing. Sources of turbulent mixing include both buoyant and shear-driven mechanisms such as convection, Kelvin Helmholtz Instability (KHI), and gravity waves. In the NAME simulations to be presented in this section, the ash layer depths simulated with the NAME control are compared to simulations in which a new space-time-varying vertical free-tropospheric diffusion scheme based on a clear air turbulence (CAT) index is included.

The space-time-varying free-tropospheric turbulence scheme represents the effect of KHI based on a CAT diagnostic, details of which are presented in Appendix A. This was used instead of the usual scheme in NAME which uses a constant subgrid turbulent diffusion in the free troposphere. Several case studies, using observed distributions of tracers, have attempted to estimate the magnitude of free-tropospheric diffusion [e.g., *Sillman et al.*, 1990; *Schumann*, 1995; *Balluch and Haynes*, 1997; *Legras et al.*, 2005] and have found that a large range of diffusion coefficients can result in agreement with observed profiles for different cases, largely because they consider very distinct meteorological situations [*Hall and Waugh*, 1997]. Thus, the observations are inconsistent with the use of spatially and temporally homogeneous diffusivity.

Figure 3 shows a typical space-time-varying vertical turbulent diffusivity field based on the CAT diagnostic at 00Z on 17 April 2010 at an altitude of 6 km. There is significant spatial variability in the field with the highest values located close to Iceland and lower values within the region of high pressure centered to the west of the UK. Compared to the control simulation in which the vertical turbulent diffusivity $K_{turb} = 1\ m^2\ s^{-1}$, the turbulent diffusivity predicted by the CAT diagnostic is generally lower, although there are patches (yellow colors) in the space-time-varying field which are an order of magnitude greater than the control value. Figure 2g shows that the overall effect of including a space-time-varying turbulent diffusivity is to reduce the ash layer depths during the early period. This results in a better match with the observed shallow ash layers than when using a constant turbulent diffusivity but also in an increased underestimation of the deepest layers. Thus, the location of increased mixing and ash clouds do not

coincide for this period of the simulation. This suggests that KHI does not result in the increased mixing necessary to generate the deepest ash layers or that the location of the ash cloud and/or increased mixing is incorrect.

It is also possible that another process, not currently included in this dispersion model, may be responsible for creating the deepest ash layers. Most of the deep ash layers are observed at three locations only. Leipzig in Germany, Ispra in Italy, and Payerne in Switzerland. Both Ispra and Payerne are located in the Alps, so potentially orographically generated gravity wave turbulence could be the cause of increased vertical mixing. Alternatively, aggregation of ash particles in the distal ash cloud may occur, resulting in an increased range of sedimentation rates and hence deeper ash clouds. However, given that the observed and modeled center of mass agrees well during this period (not shown), this suggests that increased sedimentation is not occurring in the observations. Furthermore, aggregation is not so efficient in distal regions where concentrations are generally much lower [*Costa et al.*, 2010]. During the early period of the eruption the emission heights were more variable than during the later period, suggesting that it might be more difficult to simulate ash layer depths for volcanic plumes with fluctuating plume heights. Finally, the discrepancy could be due to the small sample size as there are only 225 observed profiles during the early period.

6. Discussion and Conclusions

In this paper we have evaluated NAME simulations of ash layer depth for the period 15 April to 1 May 2010 using the distributed observations from the EARLINET lidar network. Overall, the model captures the distribution of ash layer depths well over the lidar locations when simulations are performed at very high (100 m) vertical resolution.

The excellent agreement between the NAME-simulated ash layer depths and those observed by the EARLINET lidars allowed us to use NAME to determine the dominant processes controlling ash layer depths. This study has shown that reduction in ash layer depth due to vertical wind shear and the deepening of ash layer depths due to vertical mixing are largely responsible for determining the ash cloud depth at the EARLINET sites. Conversely, the eruption source parameters (emission profile and particle size distribution) do not play a significant role in controlling the depth.

During the early stage of the eruption (15–17 April 2010) the model is able to simulate the very shallow ash layers (<1 km deep) when a space-time-varying turbulence scheme based on a clear air turbulence diagnostic is used, but the model fails to capture the very deep ash layers (>3 km deep). This could be due to missing sources of turbulence such as orographically forced gravity waves.

Appendix A: Space-Time-Varying Free-Tropospheric Turbulence Parameterization

One mechanism responsible for controlling the variation in subgrid-scale diffusion is a shear instability known as Kelvin Helmholtz Instability (KHI). KHI occurs when a large shear exists between two layers of a fluid with a stable density configuration. If the shear is large enough, the boundary can become distorted into an amplifying wave which breaks down into turbulence [*Ellrod and Knapp*, 1992; *Brown*, 1973]. Thus, large static stability can inhibit the onset of KHI unless shearing stress associated with the wind shear dominates. The nondimensional Richardson number (*Ri*) has often been used as a measure for possible turbulent conditions, since *Ri* is related to both shear and stability. *Ri* has been shown to be well correlated with turbulence using radiosonde profile data [*Anderson*, 1957]. However, the use of *Ri* in the operational forecast environment is difficult due to low vertical resolution of upper air data (typically 300–400 m) which fails to resolve the 95% of turbulent patches found to be less than 500 m deep [*Anderson*, 1957].

One way to avoid calculating *Ri* is to identify areas where *Ri* is reduced by the large-scale flow. Synoptic-scale deformation processes reduce *Ri* below its critical value, and turbulence restores *Ri* above critical value. Therefore, turbulence will decay unless *Ri* is maintained below its critical value by deformation processes.

Following the work of *Roach* [1970], *Brown* [1973] derived an expression for turbulent energy dissipation, ϵ, by assuming that turbulence (acting to increase *Ri* across a layer) works against deformation processes (acting to reduce *Ri* across a layer). Thus, turbulence will decay unless *Ri* can be maintained below its critical value by the deformation processes. Brown's parameterization takes the form

$$\epsilon = \Phi \frac{(\Delta V)^2}{24} \tag{A1}$$

where ΔV denotes the wind speed difference across a turbulent layer and Φ is a function of the synoptic-scale deformation processes and can be calculated as

$$\Phi = \left(0.3\zeta_a^2 + D_{\mathrm{sh}}^2 + D_{\mathrm{st}}^2\right)^{1/2} \quad \text{(A2)}$$

where $\zeta_a = \partial v/\partial x - \partial u/\partial y + f$ is the vertical component of absolute vorticity, $D_{\mathrm{sh}} = \partial u/\partial y + \partial v/\partial x$ is the shearing deformation, and $D_{\mathrm{st}} = \partial u/\partial x - \partial v/\partial y$ is the stretching deformation. Here u is the wind speed in the zonal (x) direction, v is the wind speed in the meridional (y) direction, and f is the Coriolis parameter.

In this paper the vertical turbulent energy dissipation, ϵ ($\mathrm{m^2\ s^{-3}}$), is calculated from the 3-D meteorological fields. ΔV depends strongly on the layer depth, and thus, we normalized to some standard depth, with ΔV approximated by the vertical wind speed gradient multiplied by 500 m. This ϵ is used to calculate the time- and space-varying turbulent eddy diffusivity, K_{turb}, which replaces the homogeneous vertical subgrid diffusion. $K_{\mathrm{turb}} = \epsilon\tau^2$ where τ is the Lagrangian timescale and is set to a constant 100 s. Figure 3 shows a typical space-time-varying vertical turbulent eddy diffusivity field.

Acknowledgments

We are grateful to the European Aerosol Research Lidar Network (EARLINET) for making their Eyjafjallajökull lidar database freely available (www.earlinet.org). We thank Marc Stringer and Alistair Gregory, at the University of Reading, for help in installing and running the NAME model. Output from the NAME model is available from the corresponding author upon request. We also thank Matthew Hort and the Dispersion Group at the Met Office for many useful discussions on this work while Helen Dacre was visiting as part of the Met Office Academic Partnership (MOAP) scheme. Natalie Harvey gratefully acknowledges funding from NERC grant NE/J017221/1 "Probability, Uncertainty and Risk in the Environment".

The Editor thanks two anonymous reviewers for their assistance in evaluating this paper.

References

Anderson, A. D. (1957), Free-air turbulence, *J. Meteorol.*, *14*, 477–494.

Ansmann, A., et al. (2011), Ash and fine-mode particle mass profiles from EARLINET-AERONET observations over central Europe after the eruptions of the Eyjafjallajökull volcano in 2010, *J. Geophys. Res.*, *116*, D00U02, doi:10.1029/2010JD015567.

Arason, P., G. N. Petersen, and H. Bjornsson (2011), Observations of the altitude of the volcanic plume during the eruption of Eyjafjallajökull, April-May 2010, *Earth Syst. Sci. Data Discuss.*, *4*, 1–25.

Balluch, M. G., and P. H. Haynes (1997), Quantification of lower stratospheric mixing processes using aircraft data, *J. Geophys. Res.*, *102*, 23,487–23,504.

Brown, R. (1973), New indices to locate clear-air turbulence, *Meteorol. Mag.*, *102*, 347–361.

Colette, A., and G. Ancellet (2006), Variability of the tropospheric mixing and of streamer formation and their impact on the lifetime of observed ozone layers, *Geophys. Res. Lett.*, *33*, L09808, doi:10.1029/2006GL025793.

Costa, A., A. Folch, and G. Macedonio (2010), A model for wet aggregation of ash particles in volcanic plumes and clouds: I. Theoretical formulation, *J. Geophys. Res.*, *115*, B09201, doi:10.1029/2009JB007175.

Dacre, H. F., et al. (2011), Evaluating the structure and magnitude of the ash plume during the initial phase of the 2010 Eyjafjallajökull eruption using lidar observations and NAME simulations, *J. Geophys. Res.*, *116*, D00U03, doi:10.1029/2011JD015608.

Dacre, H. F., A. L. M. Grant, and B. T. Johnson (2013), Aircraft observations and model simulations of concentration and particle size distribution in the Eyjafjallajökull volcanic ash cloud, *Atmos. Chem. Phys.*, *13*, 1277–1291.

Devenish, B. J., D. J. Thomson, F. Marenco, S. J. Leadbetter, H. Ricketts, and H. F. Dacre (2012), A study of the arrival over the United Kingdom in April 2010 of the Eyjafjallajökull ash cloud using ground-based lidar and numerical simulations, *Atmos. Env.*, *48*, 152–164.

Ellrod, G. P., and D. I. Knapp (1992), An objective clear-air turbulence forecasting technique: Verification and operational use, *Weather Forecasting*, *7*, 150–165.

Flentje, H., H. Claude, T. Elste, S. Gilge, U. Köhler, C. Plass-Dülmer, and W. Fricke (2010), The Eyjafjallajökull eruption in April 2010—Detection of volcanic plume using in-situ measurements, ozone sondes and lidar-ceilometer profiles, *Atmos. Chem. Phys.*, *10*, 10,085–10,092.

Grant, A. L. M., H. F. Dacre, D. J. Thomson, and F. Marenco (2013), Horizontal and vertical structure of the Eyjafjallajökull ash cloud over the UK: A comparison of airborne lidar observations and simulations, *Atmos. Chem. Phys.*, *12*, 10,145–10,159.

Hall, T. M., and D. Waugh (1997), Tracer transport in the tropical stratosphere due to vertical diffusion and horizontal mixing, *Geophys. Res. Lett.*, *24*, 1383–1386.

Haynes, P., and J. Anglade (1997), The vertical-scale cascade in atmospheric tracers due to large-scale differential advection, *J. Atmos. Sci.*, *54*, 1121–1136.

Jones, A., D. Thomson, M. Hort, and B. Devenish (2007), The UK Met Office's next-generation atmospheric dispersion model, NAME III, in *Air Pollution Modeling and Its Application XVII*, edited by C. Borrego and A.-L. Norman, pp. 580–589, Springer, New York.

Legras, B., I. Pisso, F. Lefèvre, and G. Berthet (2005), Variability of the Lagrangian turbulent diffusion in the lower stratosphere, *Atmos. Chem. Phys.*, *5*, 1605–1622.

Marenco, F., and R. J. Hogan (2011), Determining the contribution of volcanic ash and boundary layer aerosol in backscatter lidar returns: A three-component atmosphere approach, *J. Geophys. Res.*, *116*, D00U06, doi:10.1029/2010JD015415.

Marenco, F., B. Johnson, K. Turnbull, S. Newman, J. Haywood, H. Webster, and H. Ricketts (2011), Airborne lidar observations of the 2010 Eyjafjallajökull volcanic ash plume, *J. Geophys. Res.*, *116*, D00U05, doi:10.1029/2011JD016396.

Mona, L., A. Amodeo, G. D'Amico, A. Giunta, F. Madonna, and G. Pappalardo (2012), Multi-wavelength Raman lidar observations of the Eyjafjallajökull volcanic cloud over Potenza, southern Italy, *Atmos. Chem. Phys.*, *12*, 2229–2244.

Newell, R. E., Z.-X. Wu, Y. Zhu, W. Hu, E. V. Browell, G. L. Gregory, G. W. Sachse, J. E. Collins, K. K. Kelly, and S. C. Liu (1996), Vertical fine-scale atmospheric structure measured from NASA DC-8 during PEM-West A, *J. Geophys. Res.*, *101*, 1943–1960.

Newell, R. E., V. Thouret, J. Y. N. Cho, P. Stoller, A. Marenco, and H. G. Smit (1999), Ubiquity of quasi-horizontal layers in the troposphere, *Nature*, *398*, 316–319.

Pappalardo, G., et al. (2013), Four-dimensional distribution of the 2010 Eyjafjallajökull volcanic cloud over Europe observed by EARLINET, *Atmos. Chem. Phys.*, *13*, 4429–4450.

Roach, W. T. (1970), On the influence of synoptic development on the production of high level turbulence, *Q. J. R. Meteorol. Soc.*, *96*, 413–429.

Rose, W. I., G. J. S. Bluth, and G. G. J. Ernst (2000), Integrating retrievals of volcanic cloud characteristics from satellite remote sensors: A summary, *Philos. Trans. R. Soc. London, Ser. A*, *358*, 1585–1606.

Schumann, U. (1995), Direct and large eddy simulations of stratified homogeneous shear flows, *Dyn. Atmos. Oceans*, *23*, 81–98.

Schumann, U., et al. (2011), Airborne observations of the Eyjafjalla volcano ash cloud over Europe during air space closure in April and May 2010, *Atmos. Chem. Phys.*, *11*, 2245–2279.

Sillman, S., L. Logan, and S. Wofsy (1990), A regional scale model for ozone in the United States with subgrid representation of urban and power plant plumes, *J. Geophys. Res.*, *95*, 5731–5748.

Sparks, R. S. J., M. Bursik, S. N. Carey, J. A. Glbert, and L. S. Glaze (1997), *Volcanic Plumes*, John Wiley, Chichester, U. K.

Stoller, P., et al. (1999), Measurements of atmospheric layers from the NASA DC-8 and P-3B aircraft during PEM-Tropics A, *J. Geophys. Res.*, *104*, 5745–5764.

Thouret, V., J. Y. N. Cho, R. E. Newell, A. Marenco, and H. G. J. Smit (2000), General characteristics of tropospheric trace constituent layers observed in the MOZAIC program, *J. Geophys. Res.*, *105*, 17,379–17,392.